# Slip in Entangled Polymer Melts. 1. General Features

**Vijay Mhetar and L. A. Archer***

*Department of Chemical Engineering, Texas A&M University, College Station, Texas 77843*

*Received February 3, 1998; Revised Manuscript Received September 29, 1998*

ABSTRACT: Apparent violations of the no-slip boundary condition are studied using a series of narrow molecular-weight distribution polybutadiene melts ($67300 \leq \bar{M}_n \leq 650000$), subjected to plane-Couette shearing over clean silica glass surfaces. Simultaneous measurements of slip velocity and shear stress reveal several new molecular characteristics of slip in entangled polymers. log−log plots of slip velocity versus shear stress display three distinct power-law regimes: (i) A weak slip regime at low shear stresses that is characterized by extrapolation/slip lengths $b$ of the order of a few micrometers; (ii) A stick-slip regime at intermediate shear stresses marked by periodic oscillations in slip velocity and shear stress; (iii) A strong slip regime beyond a defined critical shear stress $\sigma^*$. Slip violations in this last regime are characterized by large slip velocities and massive extrapolation lengths ($b_\infty \sim 100-1500\ \mu$m). For all polymers studied the critical stress $\sigma^*$ for the weak-to-strong slip transition is found to be proportional to the plateau modulus $G_e$ of the bulk polymer, $\sigma^* \approx (0.2 \pm 0.02)\ G_e$. This finding is consistent with a shear-induced polymer disentanglement explanation for apparent slip violations in entangled polymers. Our experimental observations are also found to be in good agreement with a recently proposed scaling theory for friction and slip in entangled polymers, which assumes noninteracting surface chains. We rationalize this last result in terms of a polymer adsorption model in which a single macromolecule spontaneously attaches to numerous surface sites, yet offers a sufficiently long tail to resist relative motion of a chemically identical bulk polymer that attempts to slide over it.

## 1. Introduction

The adhesion of flowing liquids to solid boundaries, the so-called no-slip condition, is a classic assumption made by physicists and fluid mechanicians dating back at least to Stokes. Several recent experiments suggest that at high shear stresses this no-slip assumption may not be valid for entangled polymer fluids.[1,2] To investigate slip in polymers, we follow Brochard-Wyart and deGennes[3] and define the extrapolation or slip length $b$ as the distance at which the extrapolated velocity profile vanishes (see Figure 1). Thus, the slip length $b = V_s/\dot{\gamma}$ where $\dot{\gamma} = (V - 2V_s)/d$ is the shear rate corrected for slip and $V_s$ the slip velocity. For simple molecules, $b$ is typically of the order of the molecular size irrespective of the stress imposed. For entangled polymers, however, $b$ will be shown to become several orders of magnitude larger than the molecular size when stress exceeds a critical value of the order of the plateau modulus of the polymer.

Much of the recent upsurge in interest in polymer slip originates from the speculation that slip is at least partially responsible for surface instabilities commonly observed in polymer melt extrusion processes.[4−12] That these instabilities manifest as extrudate surface defects provides an economic motive for such studies. Polymer surface instabilities in extrusion are also fascinating for two other reasons. First, the instabilities are found at vanishing Reynolds numbers, which rules out the usual inertia-based instability mechanisms found in bulk Newtonian fluids. Second, the instabilities begin at the polymer−wall interface, indicating that the detailed configuration, friction, and dynamics of macromolecules near solid surfaces may play a role.

Thorough reviews describing the details of the flow behavior during polymer extrusion instability are available;[4,7] here, we only mention a few to delineate the basic features. Kalika and Denn[7] studied capillary extrusion of polyethylenes and reported a sequence of flow instabilities in detail. At a first critical stress, they observed small-amplitude, large-frequency distortion on the surface of the extrudate, commonly termed *sharkskin*. At higher stresses the pressure at the die inlet and the extrudate throughput were observed to go through periodic oscillations. At the same time, the extrudate manifested alternating regions of sharkskin and smoothness. At even higher stresses the oscillations in pressure and extrudate throughput disappeared and the extrudate was found to be grossly distorted (an observation commonly termed *melt fracture*).

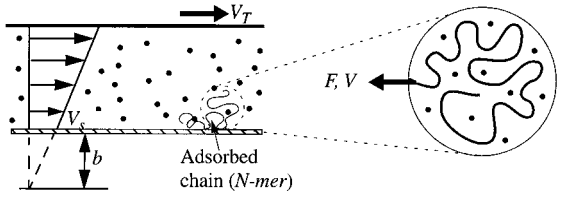


**Figure 1.** A polymer melt sheared over an ideal weakly grafted surface. There exists a finite slip velocity, $V_s$, at the polymer−wall interface. If the extrapolation length, $b \equiv V_s/\dot{\gamma}$, is much larger than the size of the grafted chain, this chain should feel the surrounding polymer molecules moving by with a uniform velocity $V_s$. In a simple paradigm to this situation we consider a probe chain pulled by one of its ends with a velocity $V = V_s$ through an entangled polymer and evaluate the friction force $F$ it experiences. At low graft densities (nonoverlapping surface chains) the shear stress at the wall is just $\sigma = \nu F$.

Vinogradov et al.[5] carried out a series of careful capillary flow experiments on a range of polybutadiene melts with varying molecular weights. Beyond a defined critical wall shear stress in the range 0.1−1 MPa, a sudden increase in throughput of the extrudate (spurt) was observed and attributed to macroscopic slip. Importantly, this behavior was found only for polymer samples with $\bar{M}_w/M_e > 5$ and the critical shear stress observed to be independent of polymer molecular weight. A similar finding was reported by Lim and Schowalter[10]

10.1021/ma980163w CCC: $15.00 
Published on Web 11/11/1998

who used a flush mounted hot-film probe to investigate apparent slip violations in a series of polybutadienes extruded through narrow capillaries. These authors found that polymer samples with $\bar{M}_w > 78000$ showed a pattern of no slip, stick slip, and macroscopic slip as the flow rate was progressively increased. The critical stress for extrudate distortion was determined to be independent of the molecular weight, corroborating the results of Vinogradov et al.[5]

Recently, Wang and co-workers[11,12] carried out extensive experiments on capillary flow of linear polyethylene melts over a wide range of experimental conditions. For bare metallic walls, they concluded that the transition from stick to slip is due a reversible coil-stretch transition of adsorbed polymer molecules, leading to their disentanglement from bulk macromolecules. Their experimental results also suggest that the magnitude of slip is strongly influenced by the entanglement density of the bulk polymer as well as by the topography of the polymer−wall interface.

More direct measurement of fluid velocity close to solid surfaces have been used to elucidate the microscopic origin of polymer slip.[13−16] Migler et al.,[13] for instance, used an evanescent wave induced fluorescence method combined with fringe pattern fluorescence recovery after photobleaching to investigate slippage of poly(dimethylsiloxane) melts in the immediate vicinity of silica glass surfaces (∼100 nm). These authors found that macroscopic slip ($b \sim 300\ \mu$m) of the type reported in the earlier extrusion studies is preceded by more microscopic slip ($b \sim 0.2\ \mu$m) over a wide range of shear rates. An abrupt transition from weak to strong slip was observed and explained by a flow-induced disentanglement mechanism.[13] More recently, Mhetar and Archer[14] used a tracer particle microscopy technique developed by Archer et al.[15] to investigate slip violations in a range of narrow molecular-weight distribution polystyrene solutions. Their results confirm that very interesting slip behavior is present in entangled polymers at shear stresses well below those required for macroscopic slip. As shown earlier by Mhetar and Archer, such microscopic slip measurements are actually quite important because they (a) provide a more comprehensive basis for evaluating theories for polymer slip and (b) allow material behavior close to the weak slip/strong slip transition to be investigated in detail.[14,16]

In the present study we use the same tracer particle velocimetry method to study apparent slip violations in entangled polybutadiene melts. Our objective is twofold: first, to investigate the detailed slip behavior of well-characterized polymer melts over a range of shear stress and, second, to evaluate the accuracy of existing theoretical models for polymer slip. This paper, the first in a series of two, is organized as follows. In the next section we review polymer adsorption and structure at solid surfaces, which we will see later is important for quantifying slip at surfaces. Following this, we summarize the predictions of a promising new scaling theory for polymer slip. Later, we present a study of apparent slippage of polybutadiene melts over bare silica glass surfaces during plane-Couette shear. Finally, we compare the experimental results with theoretical predictions as well as with those from previous polystyrene solution experiments. In the second paper to follow, we will focus in greater detail on the effect of the physical characteristics (e.g., roughness) and chemical nature (e.g., surface energy) of the wall surface on apparent slip of polybutadienes.[16]

Previous investigations of apparent slip violations in polymers have shown that slip strongly depends on the nature of the polymer segment−surface interactions.[5,17,18] These interactions may be expressed in terms of an exchange energy or binding energy which accounts for solvent/monomer release that accompanies segmental binding. Unlike small-molecule fluids, however, flexible polymer adsorption to a solid surface is not guaranteed even if segment−surface interactions are favorable. This difference is believed to be due to the large configurational entropy loss created when a macromolecule absorbs.[19] The structure of an adsorbed macromolecule is for this reason rather complicated. In the limit of "weak" adsorption, an adsorbed polymer chain consists of a number of small loops and trains (runs of segments which are in contact with the surface) and long tails (segments at the two ends of the chain which are not in contact with the surface).[20] Because this structure supports binding at numerous sites on the surface, the binding energy per chain can be rather large even though the exchange energy per site may be small.[19] The graft density of physisorbed macromolecules is for this same reason likely to be low. If the friction contribution from the loops and trains is small compared to that from the tails, an adsorbed macromolecule may therefore be approximated as an isolated, end-tethered chain for the purpose of computing the frictional drag it exerts on a bulk polymer that attempts to slide over it.

When an entangled, bulk polymer fluid is sheared over the adsorbed chains, two distinct possibilities arise: (i) If the drag force on the adsorbed chain is smaller than the desorption force, the adsorbed chain behaves as an end-grafted chain; (ii) if the drag force on the adsorbed chain is larger than the binding force between its adsorbed segments and the surface, shear-induced desorption occurs. In the first case, any slippage occurs between the bulk polymer chains and the adsorbed ones. At a given stress, the magnitude of such slippage is governed by the friction the adsorbed chains offer to the flow of bulk chains across them. Since this type of slip does not occur at the polymer/solid interface, it is here termed *apparent slip*. In the second case, slip occurs directly between a bulk polymer and the surface and is governed by the bare friction between the polymer segments and the surface. This second type of slip could therefore be termed *true slip*. For an ideal, nonadsorbing surface, slippage by the second mechanism is clearly favored. In that case the level of slip is determined by the bare friction $\eta_s/a$; massive, shear stress-independent slip lengths $b_{ideal} = (\eta_p/\eta_s)a$ would therefore be observed for well-entangled polymers. Here, $\eta_s$ and $\eta_p$ are the monomer and polymer viscosity, respectively, and $a$ the monomer size. Slip behavior of entangled polyethylene over a low-energy, nearly nonadsorbing surface appears to follow mechanism (ii), qualitatively.[21] However, much of the existing polymer slip data as well as those reported here show a clear dependence of slip velocity on wall shear stress and thus does not support slippage by mechanism (ii). We therefore focus on mechanism (i) in detail.

Consider an entangled polymer melt sheared over an ideal solid surface grafted with chemically identical chains (see Figure 1). If the extrapolation length is much larger than the average size of the polymer chain,

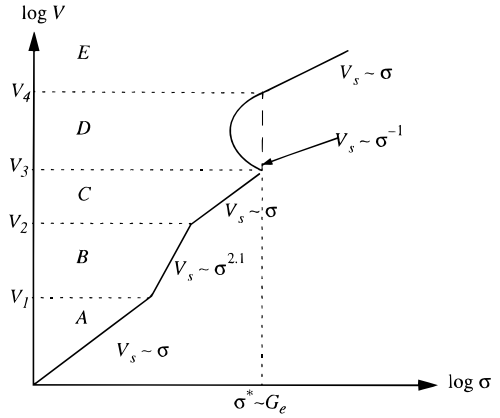


**Figure 2.** Slip velocity−shear stress diagram for an entangled polymer (*P*-mer) sheared over a weakly grafted (*N*-mer) surface. (a) Linear slip regime ($V_s < V_1 = R(N)\tau_{CR}^{-1}(N)$). (b) *Cylinder* and *ball* regime when surrounding chains are mobile ($V_1 < V_s < V_2 = D_e/\tau_{Rep}(P)$). (c) Intermediate linear slip velocity regime ($V_2 < V_s < V_3 = L_c(N)/\tau_{Rouse}(N)$). (d) Unstable regime ($V_3 < V_s < V_4 = V_3 N/N_e$). Multiple values of slip velocities exist for the same shear stress. (e) Terminal linear slip velocity regime ($V_s > V_4$).

it will feel the melt chains flowing by at the same relative velocity *V*. Brochard and de Gennes[3,22] analyzed this situation in which an entangled polymer melt flows over a weakly grafted (grafting density much smaller than the saturation density) ideal solid surface. In a more sophisticated picture, Ajdari et al.[23] estimated the friction force on a grafted polymer chain as a function of slip velocity by solving the paradigm problem of a single macromolecule pulled by one end through a bulk entangled polymer. They found that there exists a critical friction force at which a pulled/grafted polymer chain disentangles from the bulk polymer, resulting in a transition from weak slip to strong slip. Starting with the slip paradigm proposed by Ajdari et al.,[23] Mhetar and Archer[14] proposed a new scaling model for slip in entangled polymers that took into account detailed changes in configuration and relaxation dynamics of the surface chain. These authors found that the friction force exerted by a bulk entangled polymer (P monomers long, *P*-mer) on a grafted polymer chain (*N* monomers long, *N*-mer) is a strong function of the relative velocity *V*. Their predictions, for the symmetric case $N = P$ and at low grafting densities $v = 1/(Na^2)$ (i.e., nonoverlapping surface chains) can be summarized as follows (see Figure 2).

**1.1. Regime A.** At low velocities $V_s \leq R/\tau_{CR} \equiv V_1$ the surface-tethered chain is not perturbed by the moving bulk and therefore maintains its Gaussian coil configuration. Here, $R = \sqrt{N}a$ is the coil radius and $\tau_{CR}$ is the constraint release relaxation time of the grafted chain. In this regime slip velocity $V_s$ is proportional to the shear stress and slip is characterized by a constant extrapolation length $b_0 \approx Na$.

**1.2. Regime B.** For velocities above $V_1$, surface chain relaxation is frustrated and the polymer molecules begin to deform. The deformed chain splits into two sections: a relaxed Gaussian ball at the tail and a cylindrical tube at the head. In this regime the friction coefficient of the chain depends nonlinearly on the relative velocity, and the slip velocity−shear stress relation reads $\sigma \sim V_s^{1/2.1}$.

**1.3. Regime C.** When the velocity approaches $V_2 \equiv D_e/\tau_{Rep}$ the surrounding molecules act as permanent obstacles to the motion of the tethered chain. Here, $D_e = \sqrt{N_e}a$ is the average spacing between entanglements and $N_e$ is the average number of monomers between entanglements. In this regime, the tethered chain can therefore only relax by arm retraction. The slip velocity is again found to be proportional to shear stress and slippage characterized by a constant extrapolation length $b_m \equiv b_0 N/N_e = N^2 a/N_e$.

**1.4. Regime D.** When the velocity exceeds $V_3 \equiv L/\tau_{Rouse}$, retraction of the surface polymer chain is frustrated and it begins to stretch in the direction of motion (Here, $\tau_{Rouse}$ and $L = (Na)/\sqrt{N_e}$ are the longest Rouse relaxation time and contour length, respectively). This process ultimately yields a highly streamlined, sticklike surface chain configuration. The friction between the surface and bulk molecules is therefore monomeric. This regime is unstable as it results in multiple values of $V_s$ for the same $\sigma$. This regime continues until slip velocity reaches $V_4 \equiv V_3(N/N_e)$.

**1.5. Regime E.** For $V_s \geq V_4$, the friction on the probe chain is monomeric and $V_s \sim \sigma$ with huge extrapolation lengths $b_\infty = N^3 a/N_e^2$. The critical stress $\sigma_c$ for the onset of strong slip is predicted to be proportional to the plateau modulus $G_e$ of the bulk polymer.

## 2. Experimental Section

Polybutadienes were chosen as the model polymeric system for several reasons: First, polybutadienes have a low glass-transition temperature ($T_g \approx -102$ °C), facilitating room temperature experiments. Second, high-molecular-weight polybutadienes of narrow molecular-weight distribution are commercially available. Third, the low-entanglement molecular weight for polybutadienes ($M_e \approx 2100$) permits apparent slip violations to be studied over a reasonable range of entanglement densities. Fourth, with suitable hydrogenation this polymer becomes chemically similar to polyethylene, a material of considerable commercial importance in extrusion processes. We believe that the data reported here is unique in several respects: (i) The tracer particle velocimetry technique used in this study offers direct and accurate estimation of slip compared to several indirect techniques of estimating slip. (ii) Slip velocity measurements were conducted in a plane-Couette shear flow apparatus, which facilitates measurements under homogeneous shear rate conditions. (iii) The shear flow cell used here allows simultaneous measurements of motion at the walls and shear stress; it is therefore convenient for direct observation of stick-slip-type surface flow instabilities that are predicted to precede the weak slip/strong slip transition.

**2.1. Materials.** Various narrow molecular-weight distribution (MWD) polybutadienes (PBD) (1,4 addition > 90%) were purchased from Polymer Source, Inc. Weight-averaged molecular weights of the polymers used in the study ranged from $\bar{M}_w = 6.73 \times 10^4$ to $\bar{M}_w = 6.50 \times 10^5$. Detailed molecular weight and rheological properties of these materials are provided in Table 1. Polymer samples for tracer particle velocimetry measurements were prepared by first dissolving the PBD melt in toluene and then adding a small amount of 1.5-$\mu$m diameter spherical silica tracer particles to the solution. A small amount (2−5 ppm) of antioxidizing agent (Irganox 1010; Ciba-Geigy) was also added to inhibit the oxidation of PBD. The toluene was allowed to evaporate at room temperature for several days. The last traces of toluene were vacuum-evaporated at (50 °C) for about 48 h. Samples were subsequently heated in a nitrogen environment to remove any trapped air bubbles.

Prior to the slip measurements, rheological properties of all test samples were characterized by small amplitude oscillatory shearing measurements. These measurements were performed using a Paar Physica universal dynamic spectrometer (UDS), equipped with stainless steel cone-and-plate fixtures

**Table 1. Molecular Characteristics and Rheological Parameters of Polybutadiene Melts**

| sample | $\bar{M}_n$ | $\bar{M}_w/\bar{M}_n$ | $N/N_e$ | $\eta_0$ (Pa·s) | $G_e$ (Pa) | $\tau_{Rep}$ (s) |
|---|---|---|---|---|---|---|
| PBD67 | $6.730 \times 10^4$ | 1.04 | 31 | $7.53 \times 10^3$ | $7.87 \times 10^5$ | 0.022 |
| PBD86 | $8.650 \times 10^4$ | 1.04 | 40 | $1.88 \times 104$ | $7.82 \times 10^5$ | 0.058 |
| PBD129 | $1.293 \times 10^5$ | 1.03 | 60 | $7.45 \times 10^5$ | $8.25 \times 10^5$ | 0.22 |
| PBD176 | $1.764 \times 10^4$ | 1.03 | 81 | $2.03 \times 10^5$ | $8.51 \times 10^5$ | 0.57 |
| PBD253 | $2.070 \times 10^5$ | 1.04 | 95 | $3.51 \times 10^5$ | $8.69 \times 10^5$ | 0.97 |
| PBD315 | $2.850 \times 10^5$ | 1.04 | 133 | $1.07 \times 10^5$ | $8.36 \times 10^6$ | 3.07 |
| PBD650 | $5.150 \times 10^5$ | 1.05 | 239 | $7.30 \times 10^6$ | $8.35 \times 10^6$ | 22.38 |

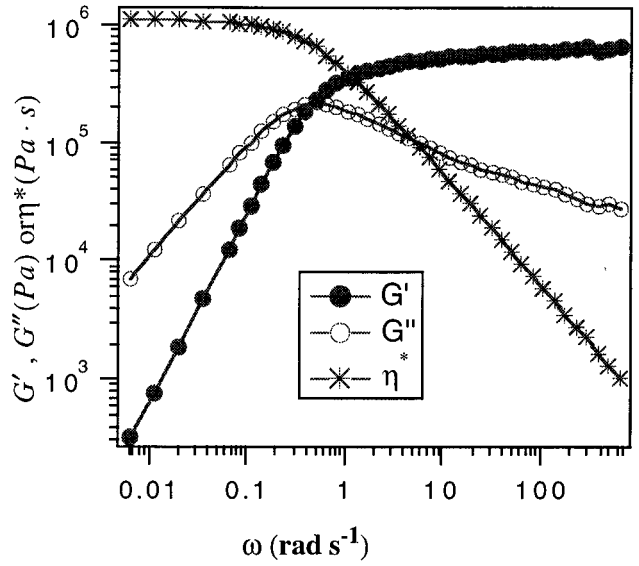


**Figure 3.** Frequency-dependent storage $G'$ and loss $G''$ moduli for the PBD253 sample. The complex dynamic viscosity vs frequency is also shown. Measurements were performed at 25 ± 0.4 °C with a strain amplitude of 7%.

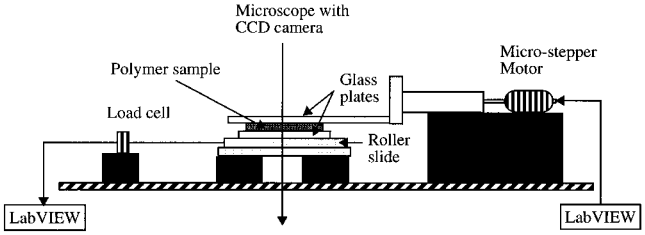


**Figure 4.** Schematic representation of the plane-Couette shear cell used for simultaneous measurements of slip velocity and shear stress. Shear flow was generated by translating the top plate relative to the bottom one. The shear force on the bottom plate was measured using a force transducer and slip velocities were inferred from the real-time motion of microscopic tracer particles observed using an optical microscope interfaced with a video camera.

(8-mm diameter; 2° cone angle). Typical frequency-dependent storage and loss modulii for PBD253 are shown in Figure 3. Rheological properties of interest deduced from these measurements are provided in Table 1. The zero shear viscosity and longest relaxation time were found to scale with the molecular weight as $\eta_0 \sim \bar{M}_w^{3.4\pm0.02}$ and $\tau_{Rep} \sim \bar{M}_w^{3.4\pm0.04}$, respectively, confirming the accuracy of the molecular-weight data and the narrowness of the molecular-weight distribution of the materials used in the study.

**2.2. Methods.** Direct measurements of slip were performed using the plane-Couette shear flow cell depicted in Figure 4. Briefly, the cell consisted of two glass plates supported by metal frames. The lower glass plate was held on a crossed roller slide as shown. A load cell (Sensotec) connected to the slide permitted the shear force acting on the lower plate to be measured. The upper glass plate was moved with the aid of a microstepper motor to impose the desired shear. The cell was designed to fit between the collimator and objective of a fixed-stage optical/fluorescent microscope capable of performing measurements with a spatial resolution of 0.5 $\mu$m. A video camera interfaced with a time lapse recorder was used to measure the time-dependent motion of tracer particles initially resting on the stationary shear cell window. Slip velocities were deduced from this information. Gaps of 250 and 500 $\mu$m were employed in all measurements. Sample aspect ratios (gap/width) never exceeded 0.02, and all tracer particle measurements were performed close to the center of the shear cell to eliminate the effects of plane-Couette secondary flow on slip measurements.[24]

An important concern in all tracer particle slip measurements is that slip can only be measured to within some unknown number of particle diameters from a surface. The error this causes in slip velocity measurements depends on the magnitude of the slip length at the conditions of the measurements. Using nanosized fluorescent tracer particles, Mhetar and Archer[14] have shown that the error in using 1.5-$\mu$m silica tracer particles is of the order of 1 $\mu$m. As we shall see later, the magnitude of slip lengths in our experiments are much greater than 1 $\mu$m; we therefore expect tracer particles to report slip lengths with sufficient accuracy for this study.

## 3. Results and Discussion

**3.1. Slip on Bare Silica Surfaces.** Slip measurements were conducted on clean silica surfaces. Cleaning was accomplished using the following three-step procedure. First, the silica surfaces were treated with freshly prepared *piranha* solution maintained at 80−100 °C for about 5 min. Piranha solution consists of a mixture of 70 parts of 30% sulfuric acid and 30 parts of 30% hydrogen peroxide. This was followed by sequential 10-min sonication cycles in acetone, 2-propanol, and methanol. A final ultrasonic cleaning and rinse with deionized (DI) water completed the cleaning protocol. The effectiveness of the cleaning procedure was evaluated by checking whether DI water completely wet the silica plates. If the plates failed this test, the procedure was repeated until complete wetting was observed.

Apparent slip velocities were deduced from the motion of tracer particles close to the stationary bottom surface. Slip velocities were determined from the long-time slope of the displacement versus time plot at different nominal shear rates $\dot{\gamma}_{app}$. Plots of slip velocity, $V_s$, as a function of shear stress, $\sigma$, for all the test samples are shown in Figure 5, parts a−g. As pointed out earlier, the shear force acting on the bottom plate was also measured. To obtain shear stress, $\sigma$, the area of the sample was computed by performing a calibration experiment at low shear rates and comparing it with shear stresses deduced from steady-shear rheometry measurements using the UDS. The measured shear stress is related to the apparent viscosity and real shear rate

$$\dot{\gamma}_{Real} = \frac{V_T - 2V_s}{d} = \dot{\gamma}_{app} - \frac{2V_s}{d}$$

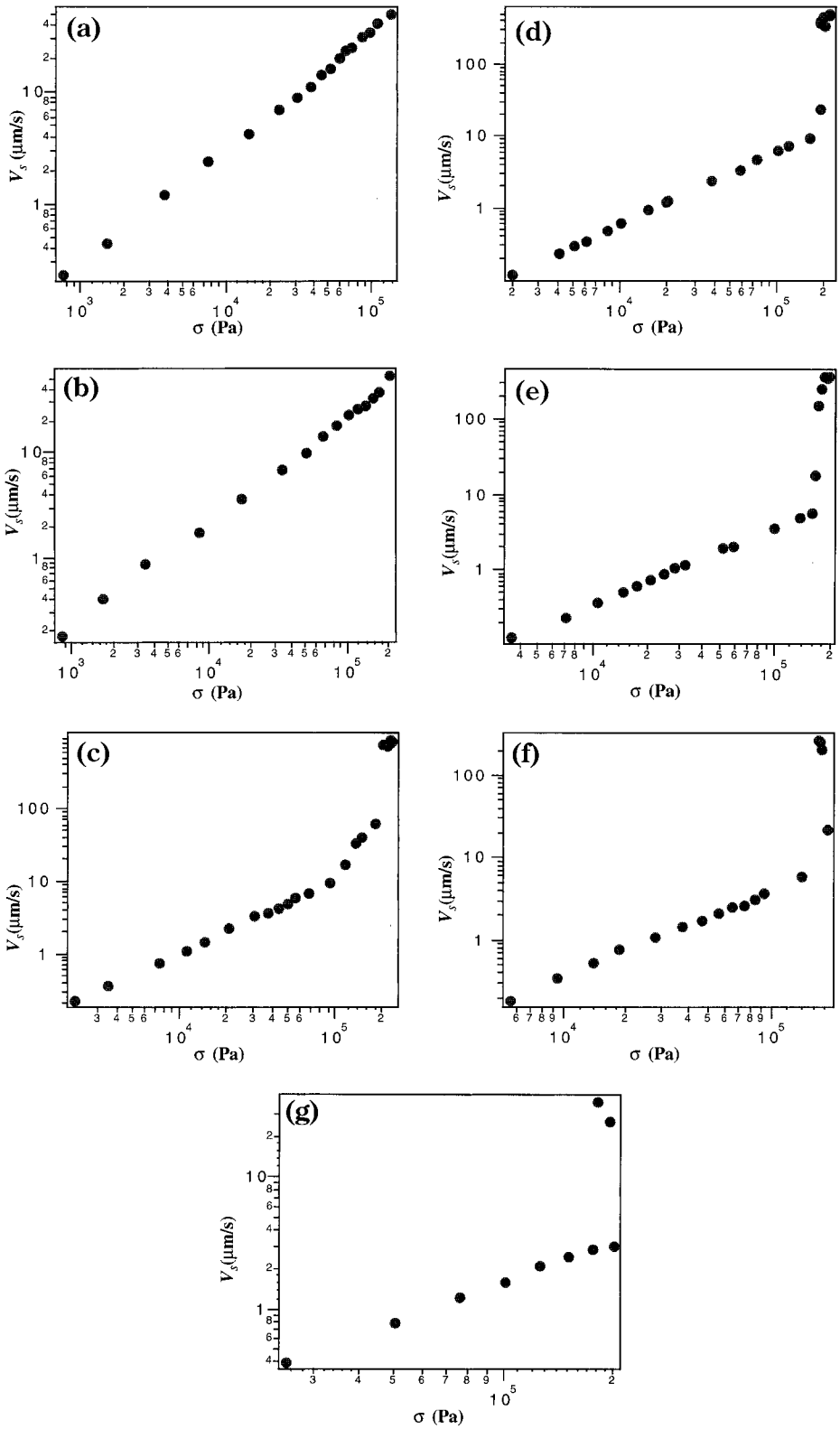


**Figure 5.** Typical plots of slip velocity ($V_s$) vs shear stress ($\sigma$) for (a) PBD67, (b) PBD86, (c) PBD129, (d) PBD176, (e) PBD253, (f) PBD315, and (g) PBD650 samples. Molecular and linear viscoelastic properties of all polymers used in the study are summarized in Table 1. Slip velocities were determined from the long-time slope of displacement vs time plots for tracer particles initially resting at the lower stationary polymer−solid interface. For samples (a) PBD67 and (b) PBD86 slip velocity is seen to be proportional to the shear stress over the entire range of shear stress studied. This slip regime is therefore characterized by a constant extrapolation length $b_0$. For samples (c)−(g), three distinct slip regimes are apparent: (i)Weak slip regime corresponding to a small slip length ($b_0$), at low stresses $\sigma < \sigma^*$; (ii) Intermediate stick-slip regime at stresses near the critical shear stress, $\sigma \approx \sigma^*$; (iii) Strong slip regime corresponding to a large extrapolation length ($b_\infty$) at stresses beyond the critical value $\sigma > \sigma^*$.

by $\sigma = \eta(\dot{\gamma}_{Real})\dot{\gamma}_{Real}$, where $V_T$ is the imposed velocity. Since these experiments (except for a small number at very high shear stresses) were performed at low real shear rates, such that $\dot{\gamma}_{Real} < 1/\tau_{Rep}$, ($\dot{\gamma}_{Real}$) may be estimated as $\dot{\gamma}_{Real} = \sigma/\eta_0$ to facilitate comparison of our $\sigma - V_s$ data with earlier $\dot{\gamma} - V_s$ results in the literature.

**Table 2. Parameters Describing Slip for the Undiluted Polybutadiene Melts**

| sample | $b_m$ ($\mu$m) | $b_\infty$ ($\mu$m) | $\sigma^*$ (Pa) | $\sigma^*/G_e$ | $V_s^*$ ($\mu$m·s$^{-1}$) | $V_{s\,Theory}^*$ ($\mu$m·s$^{-1}$) |
|---|---|---|---|---|---|---|
| PBD67 | 2.4 ± 0.22 | | | | | 262.8 |
| PBD86 | 3.5 ± 0.25 | | | | | 164.8 |
| PBD129 | 7.7 ± 0.96 | 266.5 ± 13.17 | $1.80 \times 10^5$ | 0.22 | 60.3 | 97.0 |
| PBD176 | 12.5 ± 3.26 | 398.4 ± 47.92 | $1.88 \pm 10^5$ | 0.22 | 23.1 | 67.8 |
| PBD253 | 16.3 ± 0.57 | 643.4 ± 22.34 | $1.65 \times 10^5$ | 0.19 | 17.6 | 84.3 |
| PBD315 | 39.2 ± 2.62 | 1465.5 ± 211.42 | $1.85 \times 10^5$ | 0.22 | 21.1 | 41.3 |
| PBD650 | 122.6 ± 4.79 | 1286.4 ± 387.44 | $1.88 \pm 10^5$ | 0.22 | 3.0 | 24.1 |

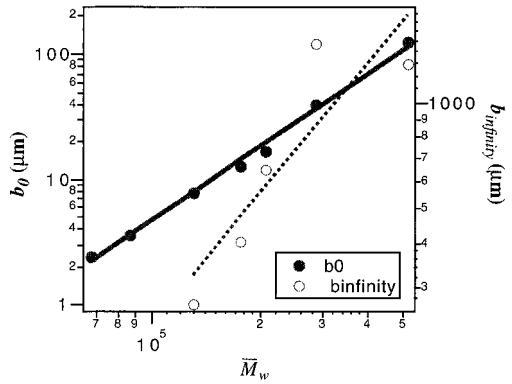


**Figure 6.** Dependence of the weak slip extrapolation length ($b_0$) and strong slip extrapolation length ($b_\infty$) on the molecular weight.

From Figure 5, parts a−g, it is apparent that the $\sigma$ versus $V_s$ plots can be subdivided into three different regimes.

*(i) Weak Slip.* At low stresses we find $V_s \sim \sigma^{1.0}$. The slip behavior in this regime can therefore be characterized by a single constant, slip length $b_m$. Experimental values of $b_m$ for all the samples studied are reported in Table 2. The small magnitude of $b_m$ indicates large friction between the polymer and surface. The results show that $b_m$ depends on the molecular weight roughly as $b_m \sim M^{1.94\pm0.07}$ (see Figure 6), which is in surprisingly good agreement with our scaling model prediction of $b_m \sim M^2$, assuming noninteracting, end-tethered surface chains. The critical shear stress $\sigma^*$ and the critical slip velocity $V^*$ at which the linear regime ceases are also provided in Table 2. The table also includes theoretical critical slip velocities, $V_s^* \approx L(N)/\tau_{Rouse}(N) = 3N^2a/(\tau_{Rep}N_e^{3/2})$. Considering the scaling nature of the slip theory and the number of assumptions needed to quantify the frictional drag experienced by surface-grafted chains, the near quantitative agreement between experimentally observed $V_s^*$ and theoretically predicted $V_s^*$ is quite remarkable. It is significant that the theoretical prediction is based on the assumption that the frictional drag offered by surface polymer molecules physisorbed from a melt to a neutral surface could be approximated by the drag produced by noninteracting end-tethered chains. The correspondence between theoretical and experimental $V_s^*$ appears to support a polymer adsorption model similar to that proposed by Semenov et al.,[20] in which *loop* radii are much smaller than the *tail* length, and the *tail* length is proportional to the adsorbed polymer molecular weight.[19]

The critical shear stress $\sigma^*$ is also seen to be proportional to the plateau modulus ($G_e$) of the samples, $\sigma^* \approx 0.2 \pm 0.02G_e$. This finding is important because it indicates that the critical stress for macroscopic slip is a material property that could be deduced from bulk rheology measurements. Simple relationships between $\sigma^*$ and $G_e$ have also been reported for other polymers using more indirect slip measurement techniques. For example, Lim and Schowalter studied slip of narrow MWD polybutadienes in slit capillary dies and found that $\sigma^* \approx 1.11G_e$. Experiments with linear low-density polyethylene solutions by Pomar et al.[25] indicate that $\sigma^* = 1.73G_e$. Vinogradov et al. found the experimental relation $\sigma^* \sim 0.4 - 0.5G_e$ from capillary flow experiments. Extrusion studies using entangled poly(dimethylsiloxanes)[26] also indicate that the critical shear stress required for the onset of macroscopic slip is essentially independent of molecular weight. These results are in reasonably good agreement with the scaling theory prediction that $\sigma^* \sim G_e$. As in the case of the critical slip velocity comparison, this finding lends support to an adsorption model wherein the adsorbed polymer's *tail* length is significantly longer than its *loop* radii. It is here useful to recall that the plateau modulus is a property of the entanglement network; as such it is virtually independent of molecular weight once polymer chains are long enough to entangle (see Table 1). The consequence of this is that for long surface chains only a relatively small error is introduced in computing $\sigma^*$ by taking $N = P$, perhaps explaining the close correspondence between the scaling theory prediction and our experimental results.

*(ii) Stick-Slip Flow.* For shear stresses slightly higher than the critical shear stress ($\sigma > \sigma^*$) a stick-slip type of instability was observed for samples with $\bar{M}_w \geq 1.29 \times 10^5$ (i.e., materials with 60 or more entanglements). For two samples, PBD67 and PBD86, this stick-slip type of instability was not observed. This finding is consistent with empirical observations by Lim and Schowalter for slip of polybutadienes in narrow slit dies. In another study, Kissi and Piau[26] observed the absence of a strong slip regime when low-molecular-weight poly(dimethylsiloxane) melts were extruded through capillary dies, in apparent agreement with our observations.

To illustrate the details of the stick-slip regime, a typical sequence of transient shear stress plots during start-up of steady shearing is presented in Figure 7, parts a−d, for the PBD315 sample. At a nominal shear rate of 0.175 s$^{-1}$ the shear stress (see Figure 7a) and corresponding slip velocity monotonically approached a steady value. At a slightly higher nominal shear rate, 0.2 s$^{-1}$, the shear stress was observed to oscillate in time, indicating the inception of the stick-slip regime (see Figure 7b). At the same time, slip velocities measured using tracer particle velocimetry were found to undergo periodic oscillations. At an even higher nominal shear rate (0.5 s$^{-1}$), the shear stress was observed to go through a maximum before commencing periodic oscillations (see Figure 7c). The stick-slip flow was characterized by the frequency of oscillations in the shear stress and slip velocity. Figure 8 shows a transient slip velocity plot during the stick-slip regime

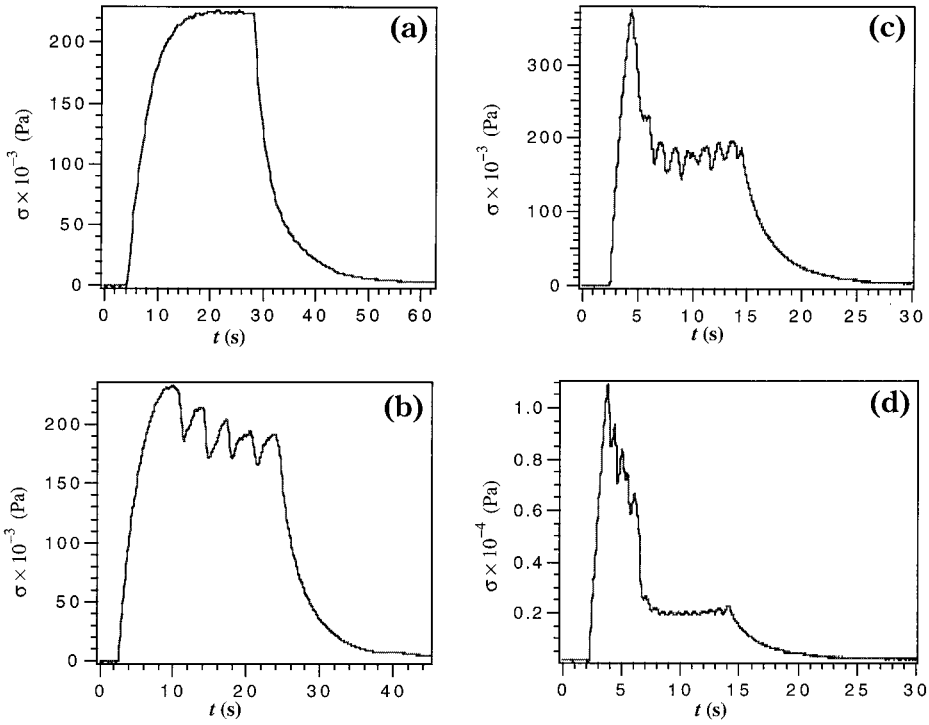


**Figure 7.** Transient shear stress response during start-up of steady shearing at several nominal shear rates. (a) At 0.175 $s^{-1}$ shear stress rises monotonically to a steady value. (b) At 0.2 $s^{-1}$ shear stress can be seen to undergo periodic oscillations. (c) At higher nominal shear rate (0.5 $s^{-1}$), the shear stress goes through a maximum before commencing periodic oscillations. Note that oscillation frequency is higher than that at the rate of 0.2 $s^{-1}$ (d) At an even higher nominal rate (1 $s^{-1}$) s the shear stress is seen to rise to a value much higher than $\sigma^* = 2.3 \times 10^5$ before undergoing large amplitude oscillation and ultimately dropping to a value close to the $\sigma^*$. The shear stress remains locked to $\sigma^*$; accordingly the oscillations in shear stress and slip velocity cease and the polymer exhibits macroscopic slip flow.

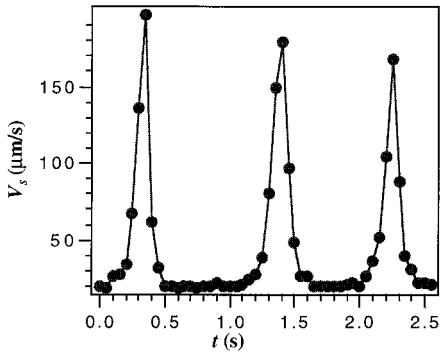


**Figure 8.** Transient slip velocities, measured from the motion of tracer particles, for PBD315 sheared at a nominal rate of 0.5 $s^{-1}$.

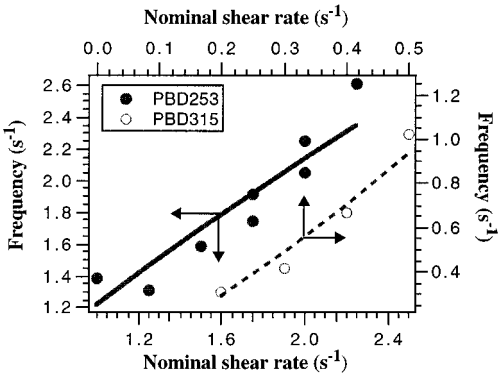


**Figure 9.** Oscillation frequency in the stick-slip regime as a function of the nominal shear rate for PBD253 and PBD315.

obtained using PBD315 sheared at a nominal rate of 0.5 $s^{-1}$. As seen in the figure, slip velocity was observed to undergo periodic weak slip−strong slip transition. Importantly, the frequency of oscillations in slip velocity (1.07 $s^{-1}$) was found to be almost identical to the frequency of the shear stress oscillations (1.03 $s^{-1}$).

As shown in Figure 9, the oscillation frequency is a function of the nominal shear rate. In fact, at low rates the frequency of oscillation is seen to be close to the inverse of the longest molecular relaxation time of the bulk polymer (for PBD253, $1/\tau_{Rep} = 1.0\ s^{-1}$; for PBD315, $1/\tau_{Rep} = 0.3\ s^{-1}$), and increases with an increasing shear rate. Both observations are important because they appear to confirm a molecular disentanglement/re-entanglement mechanism for stick-slip flow. These observations also provide further support for the recent scaling model where slip is proposed to occur by flow-induced disentanglement of surface-adsorbed and bulk polymer chains (see the Introduction section of this paper and ref 14 for more details). In this model, when the imposed shear stress reaches $\sigma^*$ surface chains disentangle from bulk ones, causing a precipitous drop in the friction force per adsorbed chain and shear stress to much lower values. At these lower stresses disentangled surface chains should re-entangle with their neighbors on a time scale of the order of $\tau_{Rouse}$. The friction force (and hence shear stress) should therefore quickly commence its increase back toward the critical value $F^*$. At low rates, $Wi \equiv \tau_{Rep}\dot{\gamma} < 1$, the time scale for the shear stress to re-approach $\sigma^*$ is of the order of the longest molecular relaxation time of the bulk chains, $\tau_{Rep}$, thus explaining the experimental observation. At high rates $Wi > 1$, the rise time for the shear stress is no longer a function of $\tau_{Rep}$, but rather it increases roughly as $\dot{\gamma}^{-1}$,[27] which is again in good agreement with our observations that the oscillation frequency increases

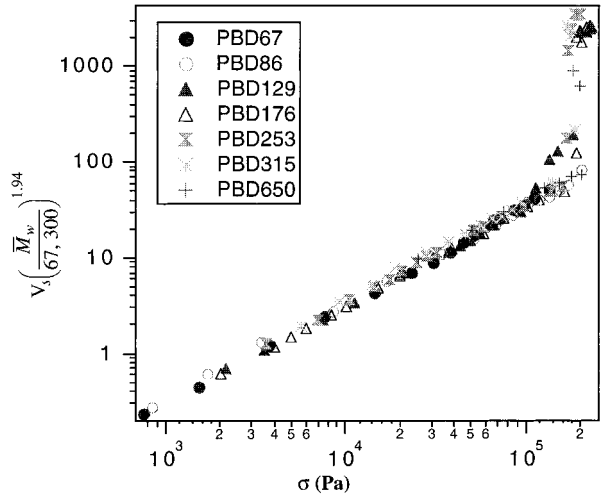


**Figure 10.** Reduced slip velocity ($V_s(\bar{M}_n/67300)^{1.72}$) versus shear stress for all PBD samples on a clean silica surface. The reference molecular weight, 67300, is that of PBD67.

with the imposed shear rate as $\dot{\gamma}^{0.8\pm0.14}$ for PBD253 and $\dot{\gamma}^{1.3\pm0.2}$ for PBD315. Recent extrusion experiments by Wang et al. using polyethylene melts also suggest that the periodicity of perturbations on the extrudate surface is indeed $\tau_{Rep}$, the longest relaxation time of the bulk polymer, again in agreement with the proposed mechanism.[12]

*(iii) Strong Slip.* At steady stresses exceeding the critical value large slip velocities were observed corresponding to large extrapolation lengths ($b_\infty \sim 100-1500$ $\mu$m). In this regime, the shear stress momentarily grew to a value much higher than $\sigma^*$ (see Figure 7d) and then displayed pronounced oscillations as it descended to a value close to the $\sigma^*$ and remained "locked" to this value. Oscillations in shear stress and slip velocity cease at this point and the polymer exhibits pure slip flow near the walls.

The measured extrapolation lengths $b_\infty$ for all the test samples are presented in Table 2. It is immediately apparent that, despite the large values of $V_s$ observed, the ultimate slip lengths measured are significantly lower than the theoretical predictions $b_\infty = N^3N_e^{-2}a$, which would be of the order of a few millimeters (20.5 mm for PBD253, for example) for the polymers used in this study. The molecular-weight dependence of the experimental $b_\infty$ is reported in Figure 6. These results show $b_\infty \sim M^{1.3\pm0.4}$, compared to the theoretical prediction of $b_\infty \sim M^3$. The cause of this discrepancy is not known, but we suspect a nonideal (higher) monomer−surface friction coefficient to be responsible for the observation. We shall address this issue in some more details in paper 2. Our experimental observation, however, is in contradiction with the finding of Wang et al.[11] that $b_\infty$ deduced from extrusion measurements using commercial low-density polyethylene samples scale with molecular weight as $b_\infty \sim M_w^{3.4}$.

Figure 10 displays a master plot obtained by superposition of stress−velocity curves for all the polybutadiene samples. The curves have been shifted vertically by an amount of $(\bar{M}_n/\bar{M}_{n,PBD67})^{1.94}$ with the reference curve being that obtained for PBD67 (Figure 5a).

**3.2. Comparison with Polymer Solution Results.** Recently, we reported slip velocity−shear stress diagrams for various entangled polystyrene solutions in diethyl phthalate (DEP) sheared over cleaned bare silica. Figure 11 shows a representative $\sigma-V_s$ plot for a solution of polystyrene ($\bar{M}_w = 2.30 \times 10^6$, $\bar{M}_w/\bar{M}_n = 1.04$) in DEP, with a concentration $c = 0.1$ g/g. Several power-law regimes are immediately apparent from the plot: (A) a linear regime at low $\sigma$ with $b_0 \sim cM$, (B) a power-law regime with $V_s \sim \sigma^{1.6}$, (C) another linear regime with $b_m \sim (cM)^2$, and (D) a strong slip regime with $V_s \sim \sigma^{5.3}$. Comparing Figure 4, parts c−g, with Figure 10 reveals that regimes A and B are missing from the polybutadiene melt $\sigma-V_s$ plots. This observation is also consistent with our slip model predictions.[14] In this model the width of regime C is of the order of $(N\tau_{Rep})/(N_e\tau_{Rouse})$ which, for the polybutadiene melts, ranges from 1000 to 87000 compared to a few tens for the polystyrene solutions. Thus, observation of regimes A and B in PBD samples would require the use of shear rates ($\dot{\gamma} < 10^{-4}$ s$^{-1}$) which is below the resolution limit of our plane-Couette shear cell. Nonetheless, for regime C the polymer solution result of $b_m \sim M^{2.0}$ is seen to be rather close to the polybutadiene melt result $b_m \sim M^{1.72}$. The critical stress for macroscopic slip in the PS solutions was found to scale with the plateau modulus as $\sigma^* \sim 2.15 \pm 0.55G_e$, which is significantly higher than the PBD melts result of $\sigma^* \approx 0.2 \pm 0.02G_e$. Also, the transition to strong slippage in the polystyrene solution is seen to be rather less abrupt than that in the PBD melts, and importantly no evidence of a stick-slip type of instability is found in the solutions.

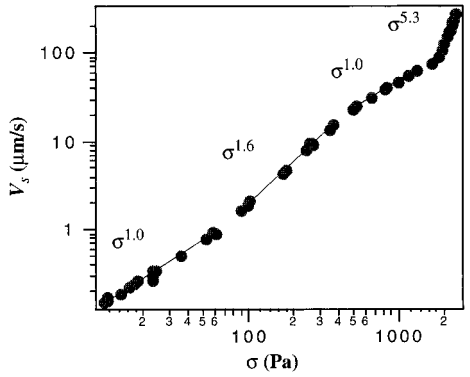


**Figure 11.** A typical slip velocity versus shear stress plot for entangled polystyrene solutions. The data here are for a 10 wt % solution of polystyrene ($\bar{M}_w = 2.12 \times 10^6$, $\bar{M}_w/\bar{M}_n = 1.04$) in diethyl phthalate.

**3.3. Estimation of Slip Using Parallel Plate Rheometry.** Recently, Henson and Mackay[28] showed that shear flow generated between parallel plates in a torsional rheometer provides a simple means of estimating the magnitude of slip in entangled polymers. This technique, originally proposed by Yoshimura and Prud'homme,[29] involves the measurement of nominal wall shear stresses at several gaps at a fixed nominal shear rate. The slip length, $b$, is then given by

$$\frac{\sigma_\infty}{\sigma(H)} = 1 + \frac{2b}{H} \qquad (1)$$

where $\sigma(H)$ and $\sigma_\infty$ are the nominal wall shear stresses at the gap $H$ and for infinite gap, respectively. We conclude this section by comparing results of our tracer particle velocimetry technique with those obtained from the more readily accessible torsional shear method of Yoshimura and Prud'homme.[29] To ensure surface conditions identical to those of the tracer particle velocimetry experiments, silica disks (25.4-mm diameter) were

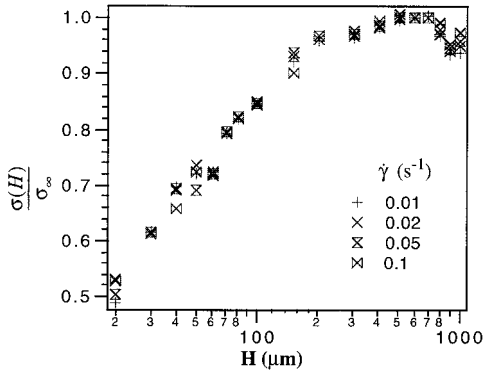


**Figure 12.** Normalized steady-state shear stress as a function of plate separation for various nominal edge shear rates, for PBD129. At large gaps ($H > 200$ $\mu$m) the shear stress is more or less independent of gap whereas at small gaps ($H < 100$ $\mu$m) the shear stress decreases strongly with a decrease in gap.

**Table 3. Comparison of Extrapolation Lengths Obtained from Parallel Disk Torsional Shear Rheometry[28] with Those From Tracer Particle Velocimetry Measurements**

| sample | $b_{m,Torsional\ shear}$ ($\mu$m) | $b_{m,Tracer\ particle}$ ($\mu$m) |
|---|---|---|
| PBD86 | $3.8 \pm 0.59$ | $3.25 \pm 0.25$ |
| PBD129 | $9.3 \pm 0.48$ | $7.7 \pm 0.96$ |
| PBD176 | $13.64 \pm 1.23$ | $12.5 \pm 3.26$ |

fixed onto the parallel plate tool of the UDS and a wide silica plate was attached to the stationary bottom plate. Prior to the experiments both silica pieces were thoroughly cleaned using the procedure described in section 3.1.

Figure 12 shows the ratio $\sigma(H)/\sigma_\infty$ plotted as a function of $H$, for four different shear rates, for the PBD129 sample. At large gaps ($H > 200$ $\mu$m) the steady-shear stress ($\sigma(H)$) was found to be more or less independent of gap, whereas at small gaps ($H < 100$ $\mu$m) $\sigma(H)$ decreases significantly with a decrease in gap. A fit of the data to eq 1 resulted in a value of ($b = 9.3 \pm 0.48$ $\mu$m) compared to $b_m = 7.7 \pm 0.96$ $\mu$m obtained by the tracer particle velocimetry measurements. Table 3 compares the slip lengths obtained by this technique to those obtained by tracer particle velocimetry for two other samples. Considering the very different nature of these experiments, the agreement is reasonable. Thus, a parallel plate viscometer operated at different gaps represents an attractive technique for estimating slip lengths in entangled polymers. The radial dependence of shear rate in parallel plate torsional shear will, however, prohibit such measurements in fluids where (a) the fluid is shear-thinning in the range of shear rates used and (b) slip is a strong function of shear stress. The precise value of the critical stress will therefore be difficult to ascertain by this method.

## 4. Summary

Apparent slip violations were studied in a series of model polybutadiene melts sheared over clean silica surfaces. log−log plots of slip velocity versus shear stress (Figure 5, parts a−g) reveal three regimes. (i) Weak slip: In this regime slip velocity was observed to be simply proportional to shear stress $V_s \sim \sigma^{1.0}$, and the extrapolation length $b$ took a constant value $b_m$ (see Table 2). The magnitude of $b_m$ was found to depend on the molecular weight as $b_m \sim M^{1.94\pm0.07}$ (see Figure 6). This result is in close agreement with the prediction ($b_m \sim M^2$) from a recently proposed scaling theory for polymer slip that assumed nonoverlapping, end-tethered surface chains. (ii) Stick slip: This regime was observed at stresses slightly above a critical value $\sigma^*$ and was marked by a stick-slip-type flow accompanied by periodic oscillations in shear stress. The stick-slip regime was seen only for samples with $\bar{M}_w \geq 1.29 \times 10^5$ (i.e., samples with 60 or more entanglements). The critical shear stress was found to be proportional to the plateau modulus of the polymers studied ($\sigma^* \approx 0.2 \pm 0.02G_e$), consistent with experimental results from several groups,[5,10,25,26] and with the prediction of a recent scaling theory for polymer slip.[14] At the inception of the stick-slip regime the frequency of oscillation was observed to be close to the inverse of the longest molecular relaxation time of the bulk polymer and to increase with increasing shear rate. These observations were explained in terms of a disentanglement /reentanglement process between surface and bulk polymer chains. (iii) Strong slip: At stresses exceeding $\sigma^*$, large slip velocities were observed and correspondingly large extrapolation lengths ($b_\infty \sim 100-1500$ $\mu$m; see Table 2) measured. The ultimate experimental extrapolation lengths were, however, significantly lower than those predicted by theory, $b_\infty = N^3N_e^{-2}a$, which is of the order of a few millimeters (e.g., 20.5 mm for PBD253), for the polymers used in the study. $b_\infty$ was also observed to scale with the polymer molecular weight as $b_\infty \sim M^{1.3\pm0.4}$, compared to that of the theoretical prediction, $b_\infty \sim M^3$. Although the cause of this discrepancy remains a mystery, we suspect that it is due to a nonideal (higher) monomer−surface friction coefficient. We shall address this issue further in the second paper.[16]

**Acknowledgment.** We are grateful to the National Science Foundation Career program and to the 3M Corporation Nontenured Faculty award program for supporting this study.

## References and Notes

(1) Denn, M. M. *Annu. Rev. Fluid. Mech.* **1990**, *22*, 13.
(2) Schowalter, W. R. *J. Non-Newtonian Fluid Mech.* **1988**, *29*, 25.
(3) Brochard-Wyart, F.; deGennes, P. G. *Langmuir* **1992**, *8*, 3033.
(4) Petrie, C. J. S.; Denn, M. M. *AIChE J.* **1976**, *22*, 209.
(5) Vinogradov, G. V.; Protasov, V. P.; Dreval V. E. *Rheol. Acta* **1984**, *23*, 46.
(6) Ramamurthy, A. V. *J. Rheol.* **1986**, *30*, 337
(7) Kalika, D. S.; Denn, M. M. *J. Rheol.* **1989**, *33*, 815.
(8) Piau, J. M.; Kissi, N. El.; Tremblay, B. *J. Non-Newtonian Fluid Mech.* **1990**, *34*, 145.
(9) Hatzikiriakos, S. G.; Dealy, J. M. *J. Rheol.* **1992**, *36*, 703.
(10) Lim, F. J.; Schowalter, W. R. *J. Rheol.* **1989**, *33*, 1359.
(11) Wang, S. Q.; Drda, P. A. *Macromolecules* **1996**, *29*, 2627; **1996**, *29*, 4115.
(12) Wang, S. Q.; Drda, P. A.; Inn, Y. W. *J. Rheol.* **1996**, *40*, 875.
(13) Migler, K. B.; Hervet, H.; Leger, L. *Phys. Rev. Lett.* **1993**, *70*, 287.
(14) Mhetar, V. R.; Archer, L. A. *Macromolecules* **1998**, *31*, 6639.
(15) Archer, L. A.; Larson, R. G.; Chen, Y.-L. *J. Fluid. Mech.* **1995**, *301*, 133.
(16) Mhetar, V. R.; Archer, L. A. *Macromolecules* **1998**, *31*, 8617.
(17) Kissi, N. El.; Leger, L.; Piau, J.-M.; Mezghani, A. *J. Non-Newtonian Fluid Mech.* **1994**, *52*, 249.
(18) Hatzikiriakos, S. G.; Dealy, J. M. *J. Rheol.* **1991**, *35*, 497; Hatzikiriakos, S. G.; Stewart, C. W.; Dealy, J. M. *Intern. Polym. Proc. VIII* **1993**, *1*, 30.
(19) Chakraborty, A. K.; Tirrell, M. *MRS Bull.* **1996**, 28.
(20) Semenov, A. N.; Bonet-Avalos, J.; Johner, A.; Joanny, J. F. *Macromolecules* **1996**, *29*, 2179.

(21) Inn, Y.-W.; Wang, S.-Q. *Phys. Rev. Lett.* **1996**, *76*, 467.
(22) Brochard-Wyart, F.; Gay, C.; deGennes, P. G. *Macromolecules* **1996**, *29*, 377
(23) Adjari. A.; Brochard-Wyart, F.; Gay, C.; deGennes, P. G.; Viovy, J. L. *J. Phys. (France)* **1995**, *5*, 491.
(24) Mhetar, V. R.; Archer, L. A. *J. Rheol.* **1996**, *40*, 549.
(25) Pomar, G.; Muller, S. J.; Denn, M. M. *J. Non-Newtonian Fluid Mech.* **1994**, *54*, 143.
(26) Kissi, N. El.; Piau, J. M. *J. Non-Newtonian Fluid Mech.* **1990**, *37*, 55.
(27) Larson, R. G. *Constitutive Equations for Polymer Melts and Solutions*; Butterworths: Boston, MA, 1988.
(28) Henson, D. J.; Mackay, M. E. *J. Rheol.* **1995**, *39*, 359.
(29) Yoshimura, A.; Prud'homme, R. K. *J. Rheol.* **1988**, *32*, 53.

MA980163W